Space Debris: from LEO to GEO

Anne LEMAITRE

naXys - University of Namur

Plan

- Space debris problematic
- Forces
- Gravitational resonances
- Solar radiation pressure (SRP)
- Shadowing effects
- Lunisolar resonances
- Numerical integrations
- Chaos
- Atmospheric drag
- Other aspects : rotation, Yarkovsky, synthetic population

Post-doc : Deleflie and Casanova, and Phd : Valk, Delsate, Hubaux, Petit and Murawiecka

principles

- Analytical formulations : toy models
- Analytical formulations : algebraic manipulator
- Numerical integrations : for short or long periods of time
- Semi-analytical : resonant or not (STELA)
- NIMASTEP (Delsate and Compère + Petit)
  - Choice of the integrator (fixed or variable step) and the perturbations (with shadows)
  - Addition of atmospheric drag + parallel
- SYMPLEC : symplectic integrator (Hubaux)

Symplectic integrator : Hubaux

Two separate parts in the dynamics A and B : 1/2 step with one, 1 step with the second, 1/2 step with one.
Most classical : SABA, SBAB (Laskar and Robutel)
Time dependent perturbation - 500 years - ephemerides Sun
Different orders : 2, 4, 6, 8

$$H(\vec{v},\Lambda,\vec{r},\theta) = H_K(\vec{v},\vec{r}) + H_{Rot}(\Lambda) + H_{geo}(\vec{r},\theta) + H_{3B}(\vec{r},\theta) + H_{SRP}(\vec{r},\theta) = A(\vec{v},\vec{r},\Lambda) + B(\vec{r},\theta)$$

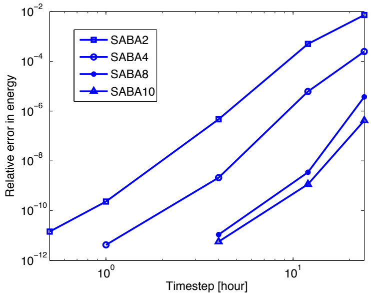

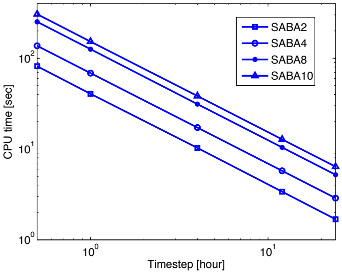

Compared with a test symplectic integrator of ESOC : LTOP

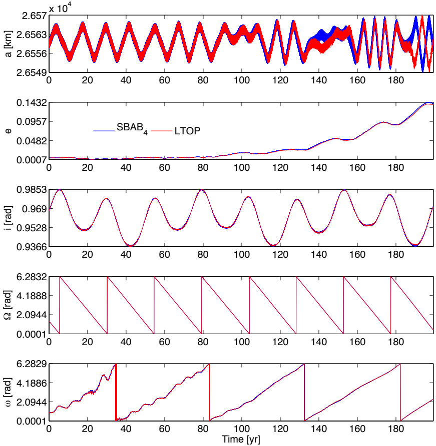

Symplectic integrator

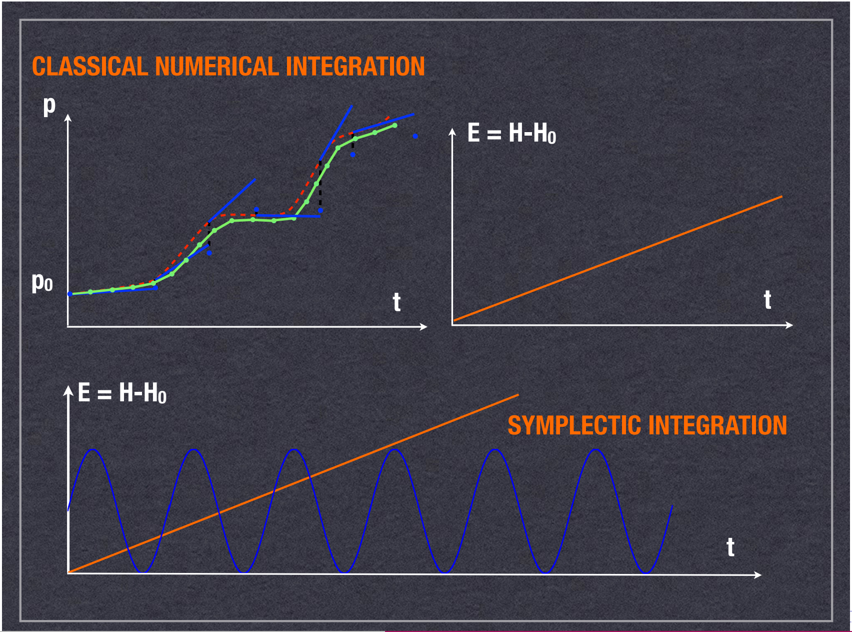

Use of several symplectic integrators

$$\dot{\vec{x}} = L_{\mathcal{H}}\vec{x} = \{\mathcal{H}, \vec{x}\} = \sum_{j=1}^{N} \left(\frac{\partial \mathcal{H}}{\partial p_j} \frac{\partial \vec{x}}{\partial q_j} - \frac{\partial \mathcal{H}}{\partial q_j} \frac{\partial \vec{x}}{\partial p_j} \right).$$

$$\vec{x}(t) = e^{\tau L_{\mathcal{H}}} \vec{x}(t_0) = \sum_{j=0}^{\infty} \frac{\tau^j}{j!} L_{\mathcal{H}}^j \vec{x}(t_0)$$

$H(p,q) = A(p,q) + B(p,q)$
$\Phi = A + B + O(\tau^{n+1})$

Yoshida 1990
S_4, S_6

$H(p,q) = A(p,q) + \varepsilon B(p,q)$
$\Phi = A + \varepsilon B + O(\tau^{2n} \varepsilon + \tau^2 \varepsilon^2)$

Laskar and Robutel 2001
$SABA_4$, $SABA_6$, $SABA_8$, $SABA_{10}$

Symplectic integrator

$$\begin{aligned}
&\mathrm{SABA}_{2n}(\tau)\\
= \; & e^{c_1\tau L_A} e^{d_1\tau L_{\varepsilon B}} \ldots e^{c_n\tau L_A} e^{d_n\tau L_{\varepsilon B}} e^{c_{n+1}\tau L_A} e^{d_n\tau L_{\varepsilon B}} e^{c_n\tau L_A} \ldots e^{d_1\tau L_{\varepsilon B}} e^{c_1\tau L_A}\\
&\mathrm{SABA}_{2n+1}(\tau)\\
= \; & e^{c_1\tau L_A} e^{d_1\tau L_{\varepsilon B}} \ldots e^{c_{n+1}\tau L_A} e^{d_{n+1}\tau L_{\varepsilon B}} e^{c_{n+1}\tau L_A} \ldots e^{d_1\tau L_{\varepsilon B}} e^{c_1\tau L_A}\\
&\mathrm{SBAB}_{2n}(\tau)\\
= \; & e^{d_1\tau L_{\varepsilon B}} e^{c_2\tau L_A} e^{d_2\tau L_{\varepsilon B}} \ldots e^{c_{n+1}\tau L_A} e^{d_{n+1}\tau L_{\varepsilon B}} e^{c_{n+1}\tau L_A} \ldots e^{d_2\tau L_{\varepsilon B}} e^{c_2\tau L_A} e^{d_1\tau L_{\varepsilon B}}\\
&\mathrm{SBAB}_{2n+1}(\tau)\\
= \; & e^{d_1\tau L_{\varepsilon B}} e^{c_2\tau L_A} \ldots e^{d_{n+1}\tau L_{\varepsilon B}} e^{c_{n+2}\tau L_A} e^{d_{n+1}\tau L_{\varepsilon B}} \ldots e^{c_2\tau L_A} e^{d_1\tau L_{\varepsilon B}}
\end{aligned}$$

Laskar & Robutel, CeMDA, 2001

Symplectic integrator

$$\mathrm{SABA}_2(\tau) = e^{c_1 \tau L_A} e^{d_1 \tau L_{\varepsilon B}} e^{c_2 \tau L_A} e^{d_1 \tau L_{\varepsilon B}} e^{c_1 \tau L_A}$$

$$\begin{aligned} \vec{x}_{k+1} &= \mathrm{SABA}_2(\tau) \vec{x}_k \\ t_{k+1} &= t_k + \tau \end{aligned}$$

$$\mathcal{H}(\vec{p}, \vec{q}) = A(\vec{p}) + \varepsilon B(\vec{q}).$$

$$\begin{aligned} \vec{x}_{k_1} &= e^{c_1 \tau L_A} \vec{x}_k \\ \vec{x}_{k_2} &= e^{d_1 \tau L_{\varepsilon B}} \vec{x}_{k_1} \\ \vec{x}_{k_3} &= e^{c_2 \tau L_A} \vec{x}_{k_2} \\ \vec{x}_{k_4} &= e^{d_1 \tau L_{\varepsilon B}} \vec{x}_{k_3} \\ \vec{x}_{k+1} &= \vec{x}_{k_5} = e^{c_1 \tau L_A} \vec{x}_{k_4} \\ t_{k+1} &= t_k + \tau. \end{aligned}$$

Symplectic integrator

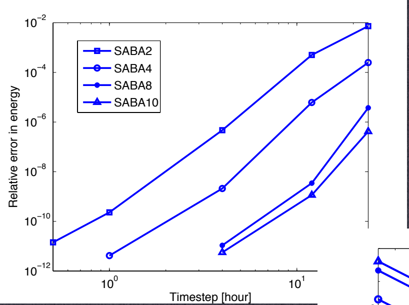

Implementation of several cases up to order 10

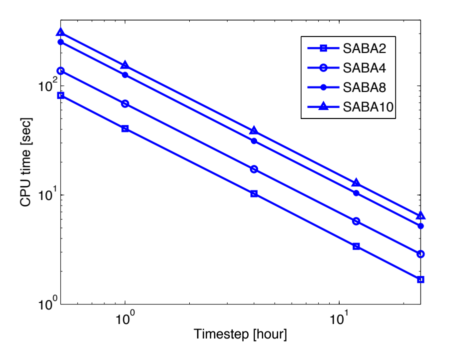

Symplectic integrator

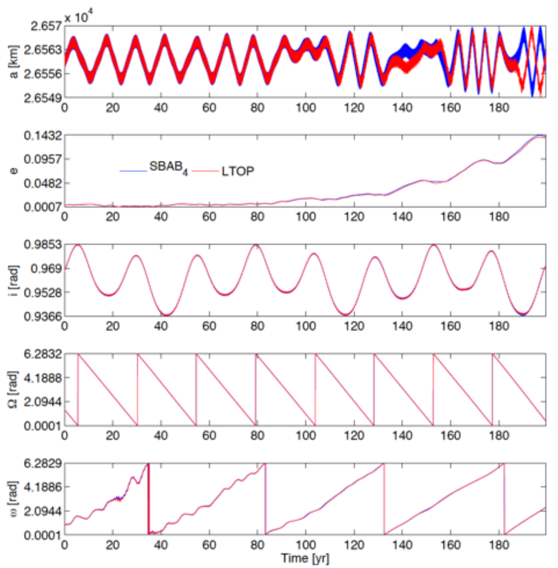

LTOP
$SBAB_4$

200 years

LTOP =
Symplectic integrator of ESA
(non public, Yoshida type)

Symplectic integrator

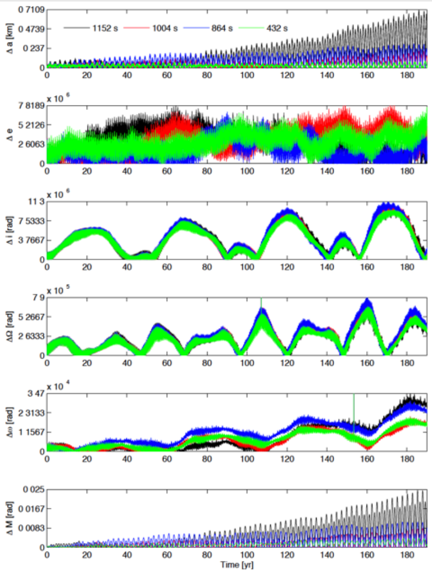

Comparisons with non symplectic integrators

Stepsize for $SABA_4$ = 4 hours = 14 400 s

stepsize for NIMASTEP = 1152 s
stepsize for NIMASTEP = 1004 s
stepsize for NIMASTEP = 864 s
stepsize for NIMASTEP = 432 s

NIMASTEP ABM 10
Adams - Bashforth - Moulton

Hubaux et al, ASR, 2012
Delsate and Compère, A&A, 2012

Symplectic integrator

OBSERVATIONAL DATA

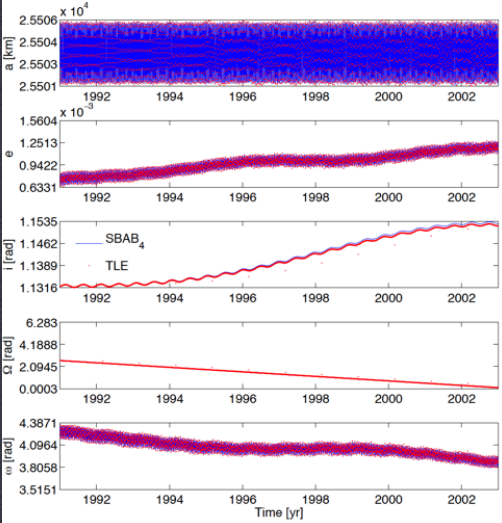

ETALON 1

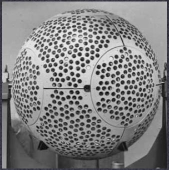

12 YEARS

motion of a TLE - MEO
integration with $SABA_4$
and by Rossi's software

Geopotential
up to degree and order 20

SRP (A/M = 0.001 m^2/kg
+ conical shadows

Sun and Moon

Passage in the Earth's shadow

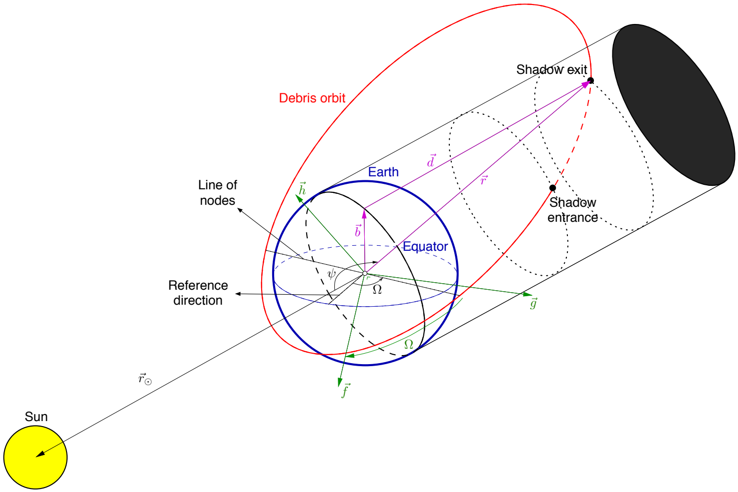

Smooth Shadowing effects

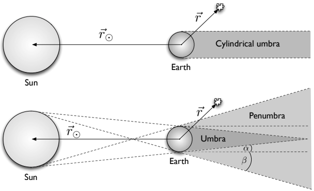

$$s_C(\vec{r}) = \sqrt{r^2 - R_\oplus^2} + \frac{\vec{r}\bullet\vec{r}_\odot}{r_\odot} \leq 0$$

switch on/off (numerically ?)

adapted averaging methods

$$\nu_C = \frac{1}{2}(1 + \tanh(\gamma\, s_C(\vec{r}))) \simeq \begin{cases} 0 & \text{in cylindrical umbra} \\ 1 & \text{otherwise} \end{cases}$$

Penumbra/umbra function for the conical case (ν_p) with 2 parameters

Gamma parameter

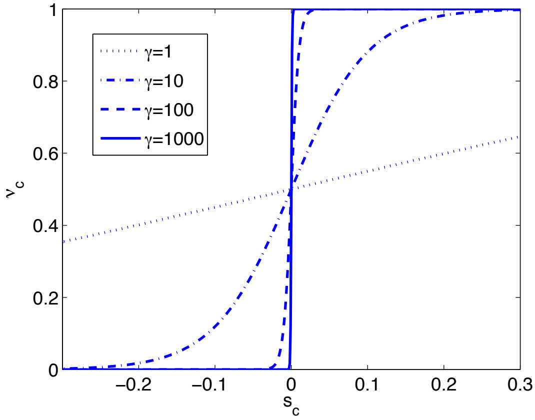

Cone

$$\alpha = \operatorname{atan} \frac{R_\odot - R_\oplus}{\|\vec{r} - \vec{r}_\odot\|} \quad \text{and} \quad \beta = \operatorname{atan} \frac{R_\odot + R_\oplus}{\|\vec{r} - \vec{r}_\odot\|}$$

with $R_\odot$ the radius of the Sun. Extending relation (3.7), it follows that space debris are in the umbra cone when

$$s_{\mathrm{u}}(\vec{r}) := \frac{\vec{r} \cdot \vec{r}_\odot}{r_\odot} + \cos\alpha \left[\sqrt{r^2 - R_\oplus^2 \cos^2\alpha} + R_\oplus \sin\alpha \right] \leq 0$$

and in the penumbra cone when

$$s_{\mathrm{p}}(\vec{r}) := \frac{\vec{r} \cdot \vec{r}_\odot}{r_\odot} + \cos\beta \left[\sqrt{r^2 - R_\oplus^2 \cos^2\beta} - R_\oplus \sin\beta \right] \leq 0.$$

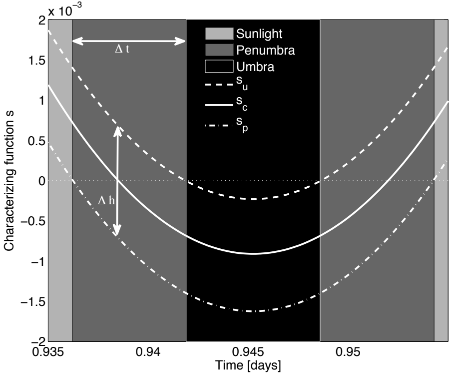

FIGURE 3.4 • *Evolution of the functions s_c, s_u and s_p during a shadow crossing on a geostationary orbit. The penumbra and umbra cones are crossed respectively when s_p is negative and s_u is negative. The time spent in the penumbra transition is noted Δt and the difference between s_u and s_p at the entrance of the cylindrical shadow is denoted by Δh.*

Smooth Shadowing effects

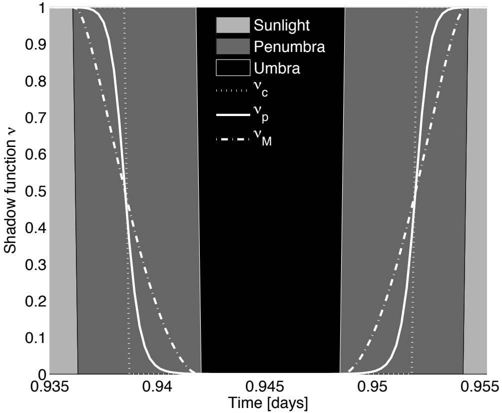

ν_M proposed by Montenbruck and Ghill (2005)

Chaos

- Use of the usual chaos indicators
- MEGNO : Mean Exponential Growth factor of Nearby Orbits (Cincotta and Simo)
- Integrated with NIMASTEP and symplectic integrator
- Frequency Map (Laskar)
- Important information for the validity of the integrations and detection of stability areas
- Other studies : FLI

Quantitative consideration: Indicators of chaoticity

In chaotic (irregular) regions of phase space two initially nearby trajectories **separate roughly exponentially with time**; in quasi-periodic (regular) neighboring trajectories **separate roughly linearly with time** (Chirikov, 1979)

Consequences:

- Computation of rate of separation (divergence)
- Sensitive dependence on initial conditions

Rate of divergence - Variational methods

Definition

$$\gamma = \frac{1}{t - t_0} \ln\left(\frac{d(t)}{d(t_0)}\right)$$

d is the Euclidian distance between two initially nearby trajectories.

- Chaotic trajectories (irregular):
  d grows exponentially (on the average), γ approaches some positive constant
- Quasi-periodic trajectories (regular):
  d grows linearly, γ approaches zero as $ln(t)/t$

$$\frac{d}{dt}\boldsymbol{x}(t) = \boldsymbol{f}(\boldsymbol{x}(t), \alpha), \qquad \boldsymbol{x} \in \mathbb{R}^{2n}$$

where α is a vector of parameters

$$\dot{\delta} = \frac{d}{dt}\delta(\phi(t)) = \boldsymbol{J}(\phi(t))\,\delta(\phi(t)), \quad \text{with} \quad \boldsymbol{J}(t) = \frac{\partial \boldsymbol{f}}{\partial \boldsymbol{x}}((\phi(t))),$$

with $\delta = x(t) - x_0(t)$ and $\phi(t)$ is a solution of the flow.

The Lyapounov Characteristic Number λ (LCN)

$$\lambda = \lim_{t\to\infty} \lambda_1(t), \quad \text{with} \quad \lambda_1(t) = \frac{1}{t}\ \ln \frac{\|\delta(\phi(t))\|}{\|\delta(\phi(t_0))\|}$$

The MEGNO indicator - Integral formulation

$$\lambda = \frac{1}{t} \int_0^t \frac{\dot{\delta}(\phi(s))}{\delta(\phi(s))}\, ds$$

where $\delta = \|\boldsymbol{\delta}\|$, $\dot{\delta} = \dot{\boldsymbol{\delta}} \cdot \boldsymbol{\delta}/\delta$.

MEGNO

The **M**ean **E**xponential **G**rowth factor of **N**earby time-weighted version of the integral form of the LCN. More precisely, Cincotta et al. introduced and defined the MEGNO indicator:

$$Y(\phi(t)) = \frac{2}{t} \int_0^t \frac{\dot{\delta}(\phi(s))}{\delta(\phi(s))}\, s\, ds, \qquad \overline{Y}(\phi(t)) = \frac{1}{t} \int_0^t Y(\phi(s))\, ds$$

The MEGNO indicator - properties

- Chaotic (irregular)
  $\overline{Y}(t) \simeq \lambda/2\ t$
- Quasi-periodic (regular)
  $\overline{Y}(t) \to 2$
- Stable, isochronous periodic orbits $\overline{Y}(t) \to 0$

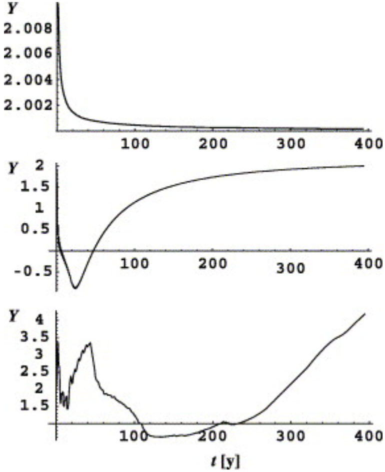

Breiter et al 2001

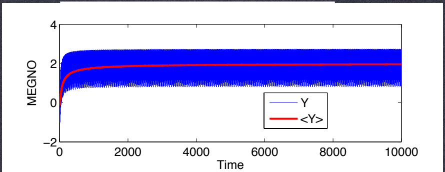

Stable quasi-periodic orbit

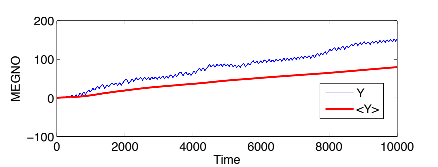

Unstable orbit

time in days

MEGNO

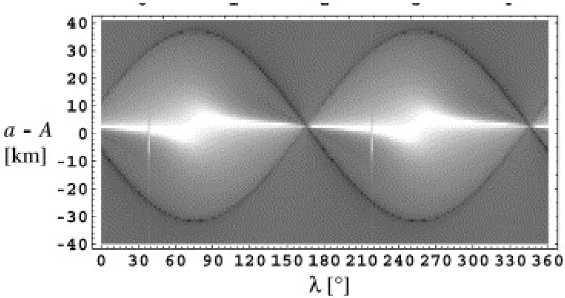

40
30
20
10
0
-10
-20
-30
-40
a - A
[km]
0 30 60 90 120 150 180 210 240 270 300 330 360
λ [°]

Chaos maps

MEGNO : GEO - 30 years - $A/M = 1, 5, 10, 20\ m^2/kg$

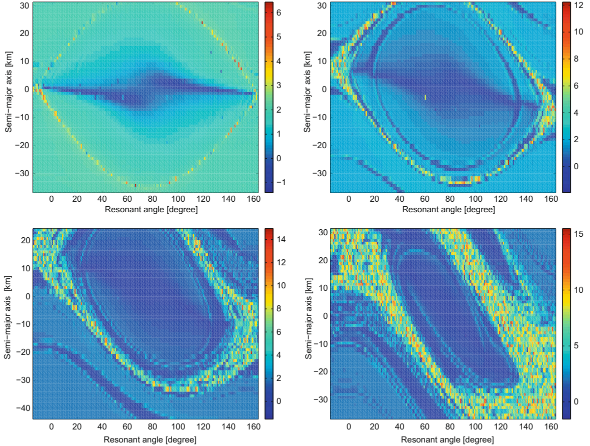

Geo resonance

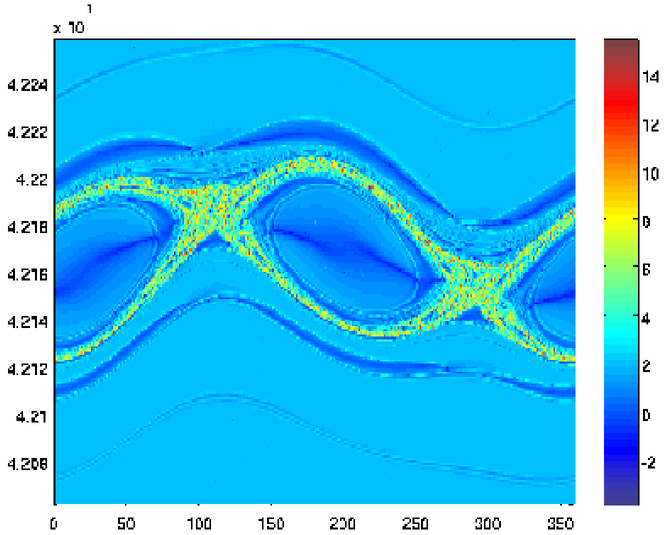

Geo resonance

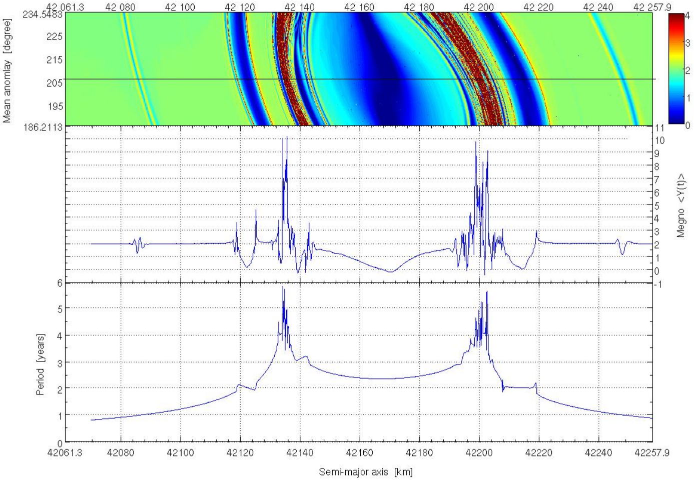

Variation of the frequencies - second derivatives

Principle

The main purpose of the FAM is to determine the approximation $f'(t)$ of a signal $f(t)$, where both are developed in Fourier series:

$$f'(t) = \sum_{k=1}^{N} p'_k e^{\imath \nu'_k t} \text{ approximation of the initial signal } f(t) = \sum_{k=1}^{\infty} p_k e^{\imath \nu_k t}.$$

The frequencies ν'_k for $k = 1, \ldots, N$ and their associated decreasing amplitudes p'_k for $k = 1, \ldots, N$ are determined through an iterative scheme.

Frequency map

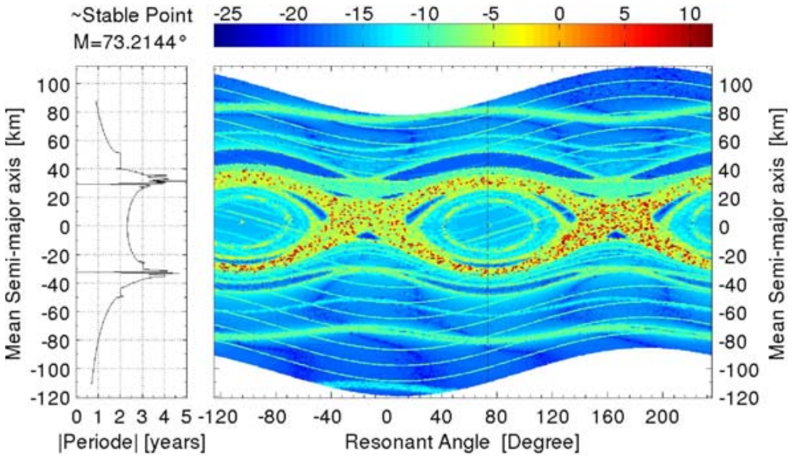

Further analysis stability

Primary and secondary resonance analysis : stability zones

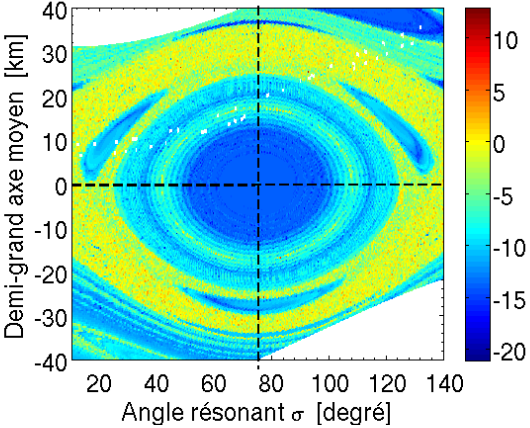

Secondary resonances

Hamiltonian

$$\mathcal{H} = -\frac{\mu^2}{2L^2} - \dot{\theta} L + \frac{\mu}{a^3}\, R_e^2\, (F_{200}(i)\; G_{200}(e)\; S_{2200} + F_{221}(i)\; G_{212}(e)\; S_{2212})$$

Truncation

$$\mathcal{H} = -\frac{\mu^2}{2L^2} - \dot{\theta} L + \frac{3\mu^4}{L^6} R_e^2\; J_{22} \cos 2(\sigma - \sigma_0) - \frac{15\mu^4}{2L^6} R_e^2\; e^2\; J_{22} \cos 2(\sigma - \sigma_0).$$

$\mathcal{Z} = \kappa = \frac{3}{2}\, C_r\, P_r\, \frac{A}{m}\, \frac{a}{\sqrt{L}}$

$$\begin{aligned} x_1 &= -\kappa\ \sin\lambda_\odot + C_x &&= -\kappa\,(\sin\lambda_\odot - D_x) \\ y_1 &= \kappa\ \cos\lambda_\odot\ \cos\epsilon + C_y &&= \kappa\,(\cos\lambda_\odot\ \cos\epsilon + D_y). \end{aligned}$$

Resonance

$$e^2 = \frac{\mathcal{Z}^2}{L^2 n_S^2} + \gamma^2 + \frac{2\mathcal{Z}}{L n_S}\gamma \cos(\lambda_S + \delta)$$

and the final (with all these successive approximations) Hamiltonian K is:

$$K(L,\sigma) = -\frac{\mu^2}{2L^2} - \dot{\theta} L + \cos(2\sigma - 2\sigma_0)\left[\frac{F}{L^6} - \frac{2G}{L^6}\cos(\lambda_S + \delta)\right],$$

with

$$F = 3\mu^4 R_e^2 J_{22} - \frac{15\mu^4}{2} R_e^2 J_{22}\left(\frac{\mathcal{Z}^2}{L^2 n_S^2} + \gamma^2\right)$$

$$G = \frac{15\mu^4}{2} R_e^2 J_{22}\frac{\mathcal{Z}}{L n_S}\gamma$$

Secondary resonances

Resonance

$$
\begin{aligned}
K &= -\beta \left(\frac{R^2}{2} - b \, \cos r \right) - 2 \frac{G}{L_0^6} \, \cos r \cos\left(\lambda_S + \delta\right) \\
&= -\beta \left(\frac{R^2}{2} - b \, \cos r + 2 \, G' \, \cos r \cos \eta \right) \quad \text{with } G' = -\frac{G}{\beta L_0^6} \\
h &= \frac{K}{-\beta} = \frac{R^2}{2} - b \, \cos r + G' \, \cos\left(r + \eta\right) + G' \, \cos\left(r - \eta\right),
\end{aligned}
$$

where $\eta = \lambda_S + \delta$.

Circulation cases

Fig. 6 Circulation case: The periods of $\sigma - \sigma_0 = \frac{r}{2}$ calculated in years, as functions of the distance (*in kilometers*) from the separatrix, calculated for $r = 0$ and $R = \rho$, obtained analytically (*line*) by Eq. 20 and by a numerical integration of the pendulum differential equations (*dots*)

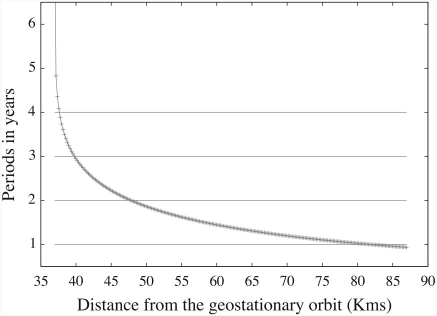

Secondary resonances

Libration cases

Fig. 4 Libration case: The period T (*in years*) calculated by a numerical integration of the pendulum differential equations (*dots*) and through the analytical expressions (*lines*), as functions of ϵ in the libration zone; ϵ is an angle measured from the separatrix

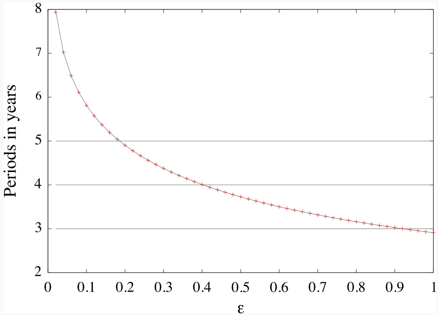

Three values of Φ : 60.26°, 180.26°,and 300.26°, , measured from the vertical positive axis on which $\Phi = 0° = r$. .

Initial map

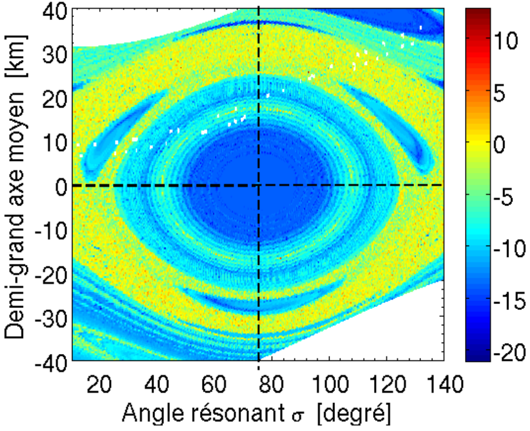

Demi-grand axe moyen [km]
40
30
20
10
0
-10
-20
-30
-40
20
40
60
80
100
120
140
Angle résonant σ [degré]
10
5
0
-5
-10
-15
-20

Long term evolution

Libration cases

Fig. 8 Evolution of the resonant angle $2(l-\theta)+\lambda_s$. The used model is the numerical model of Fig. 2, involving a long supplementary period of 150 years. The initial conditions are the same of the Fig. 2 with $M = 199.8°$

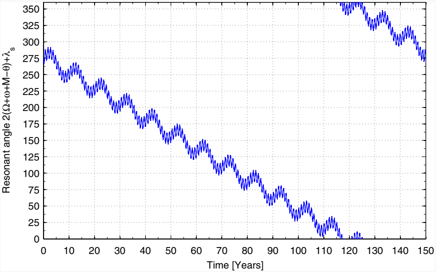

Regular case : without shadow

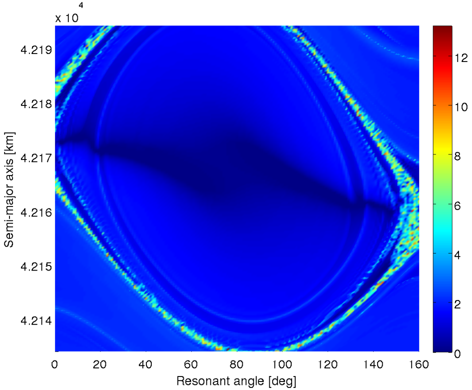

Figure 5.12 • *Stability analysis of the two-dimensional plane* (σ_{res}, a) *represented using MEGNO values at* 30 *yr without Earth's shadows. A set of* 160×160 *uniformly distributed initial conditions has been integrated with* S_4 *with time steps equal to* 0.05 *day*$/2\pi$. *Other initial conditions are fixed to* $e = 0.002$, $i = 0.004$ *rad and* $\Omega = \omega = 0$ *rad. The value of the initial sidereal time* θ *is determined by the initial time epoch at* 25 *January* 1991. *The model includes the central body attraction, the geopotential up to degree and order* 2, *luni-solar perturbations and SRP with the AMR equal to* 5 m^2/kg. *Same representation as in Valk et al. (2009)*

Regular case : different times

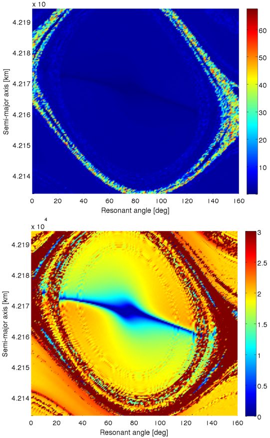

Figure 5.13 • *Stability analysis of the two-dimensional plane* (σ_{res}, a) *represented using real (top) and cut off (bottom) MEGNO values at* 300 *yr without Earth's shadows. A set of* 160×160 *uniformly distributed initial conditions has been integrated with* S_4 *with time steps equal to* 0.05 *day*/2π. *Other initial conditions are fixed to* $e = 0.002$, $i = 0.004$ *rad and* $\Omega = \omega = 0$ *rad. The value of the initial sidereal time* θ *is determined by the initial time epoch at* 25 *January* 1991. *The model includes the central body attraction, the geopotential up to degree and order* 2, *luni-solar perturbations and SRP with the AMR equal to* 5 m^2/kg.

With and without chaos

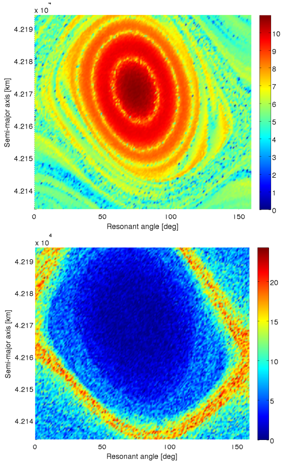

FIGURE 5.15 • *Stability analysis of the two-dimensional plane* (σ_{res}, a) *represented using MEGNO values at* 30 *yr (GSI) with Earth's shadows. Other initial conditions and integrator are chosen as in Fig. 5.12 with time steps equal to* 0.01 *day*$/2\pi$. *The model includes the central body attraction, the geopotential up to degree and order* 2, *luni-solar perturbations and SRP with the AMR equal to* 5 m^2/kg *with cylindrical (top) and conical (bottom) Earth's shadows.*

Other chaos indicators and research

- FLI : Fast Lyapounov Indicator (Froeschlé, Lega, Guzzo, etc)
- intensively used by Celletti and collaborators

International Journal of Non-Linear Mechanics 90 (2017) 147–1

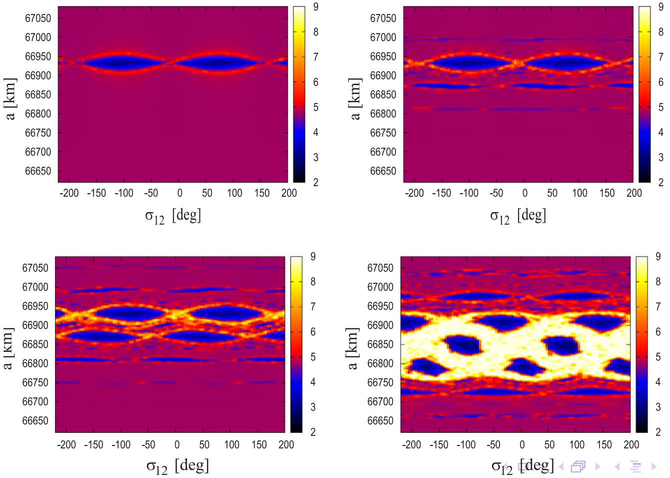

Celletti and Gales : 1:1

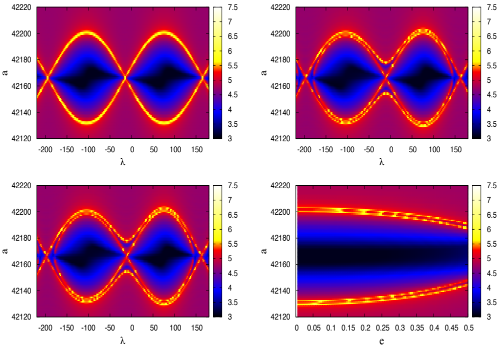

FIGURE 3. FLI (using Hamilton's equations) for the GEO 1:1 resonance for $e = 0.005$, $i = 0^o$, $\omega = 0^o$, $\Omega = 0^o$ under the effects of the J_2 and J_{22} terms (top left); all harmonics up to degree and order $n = m = 3$ (top right); all harmonics up to $n = m = 4$ (bottom left). The bottom right panel yields the FLI for $i = 0^o$, $\lambda = 75.07^o$ in the (e, a) plane under the effects of all harmonics up to $n = m = 4$.

Celletti and Gales : 1:1

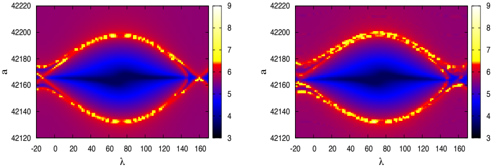

FIGURE 5. FLI (using Cartesian equations) for the GEO 1:1 resonance for $e = 0.005$, $i = 30^o$, $\omega = 0$, $\Omega = 0$, under all harmonics up to degree and order three (left panel), all harmonics up to degree and order three + Moon + Sun+ SRP with $A/m = 0.1$ (right panel).

Celletti and Gales : 2:1

Terms of the geopotential : 2:1

$$
\begin{aligned}
t_1 &= \frac{\mu_E R_E^2 J_{22}}{a^3}\left\{\frac{3}{4}(1+\cos i)^2\left(-\frac{e}{2}\right)\cos(\sigma+\omega-2\lambda_{22})\right\} \\
t_2 &= \frac{\mu_E R_E^2 J_{22}}{a^3}\left\{\frac{3}{2}\sin^2 i\left(\frac{3}{2}e\right)\cos(\sigma-\omega-2\lambda_{22})\right\} \\
t_3 &= \frac{\mu_E R_E^3 J_{32}}{a^4}\left\{\frac{15}{8}\sin i(1-2\cos i-3\cos^2 i)\left(1+2e^2\right)\sin(\sigma-2\lambda_{32})\right\}
\end{aligned}
$$

where $\sigma = 2\lambda$ with λ as in (3.14).

Celletti and Gales : 2:1

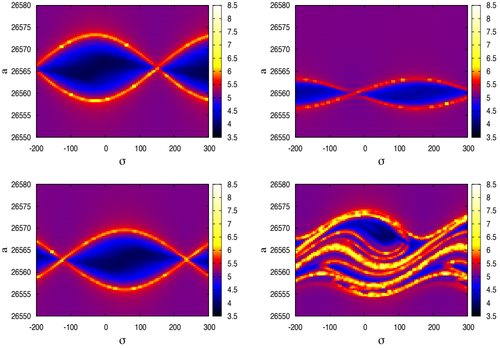

FIGURE 7. FLI for the toy–model (5.1), for $e = 0.1$, $i = 20^o$, $\omega = 0$, $\Omega = 0$, under various effects: $J_2 + t_1$ (top left); $J_2 + t_2$ (top right); $J_2 + t_3$ (bottom left); $J_2 + t_1 + t_2 + t_3$ (bottom right).

Celletti and Gales : 2:1

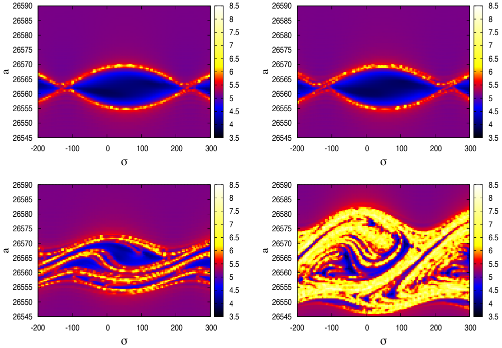

FIGURE 9. FLI (using Hamilton's equations) for the MEO 2:1 resonance, under the effects of all harmonics up to degree and order $n = m = 4$, for $i = 30^o$, $\omega = 0$, $\Omega = 0$: $e = 0.005$ (top left); $e = 0.01$ (top right); $e = 0.1$ (bottom left); $e = 0.5$ (bottom right).

Celletti and Gales : 2:1

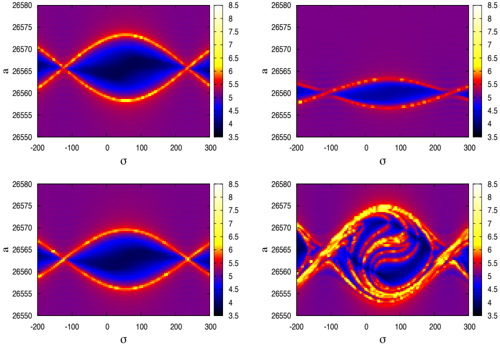

FIGURE 11. FLI for the toy–model (5.1), for $e = 0.1$, $i = 20^o$, $\omega = -85^o$, $\Omega = 0$, under various effects: $J_2 + t_1$ (top left); $J_2 + t_2$ (top right); $J_2 + t_3$ (bottom left); $J_2 + t_1 + t_2 + t_3$ (bottom right).

Lunisolar resonances

- Gravitational resonances : between the rotation of the Earth and the period of space debris
- Not to be confused with spin-orbit resonances (rotation and orbit of the same body)
- Secondary resonances : inside a resonance with another angle (between σ and $\lambda_{\odot}$
- Lunisolar resonances : secular resonances between ω and Ω of space debris and nodes and perigee of the Moon and the Sun
- Breiter, *Lunisolar resonances revisited*, CM&DA, 2001

Celest Mech Dyn Astr
DOI 10.1007/s10569-015-9665-9
ORIGINAL ARTICLE

The dynamical structure of the MEO region: long-term stability, chaos, and transport

Jérôme Daquin[1,3] · Aaron J. Rosengren[2] · Elisa Maria Alessi[2] · Florent Deleflie[3] · Giovanni B. Valsecchi[2,4] · Alessandro Rossi[2]

$$\text{For the Moon} \;:\; \dot{\Psi}_{2-2p,m,\pm s} = (2-2p)\,\dot{\omega} + m\dot{\Omega} \pm \dot{\Omega}_M \simeq 0$$

and

$$\text{For the Sun} \;:\; \dot{\Psi}_{2-2p,m} = (2-2p)\,\dot{\omega} + m\dot{\Omega} \simeq 0$$

$$\dot{\omega} = \frac{3}{4} J_2 n \left(\frac{R}{a}\right)^2 \frac{5\cos^2 i - 1}{(1-e^2)^2},$$

$$\dot{\Omega} = -\frac{3}{2} J_2 n \left(\frac{R}{a}\right)^2 \frac{\cos i}{(1-e^2)^2},$$

Breiter results

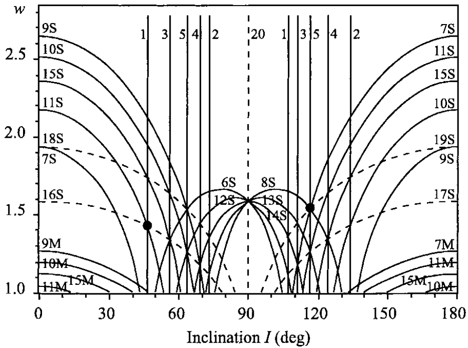

Figure 1. Location of the lunisolar resonances in the (I, w) plane. Dashed lines indicate inclination resonances.

Fig. 1 The location of resonance centers of the form $\dot{\psi}_{2-2p,m,\pm s} = (2-2p)\dot{\omega} + m\dot{\Omega} \pm s\dot{\Omega}_M = 0$, where only the effects of the J_2 perturbation on ω and Ω have been considered (adapted from Rosengren et al. 2015). These resonances form the dynamical backbone of the phase space, organizing and controlling the long-term orbital motion of MEO satellites

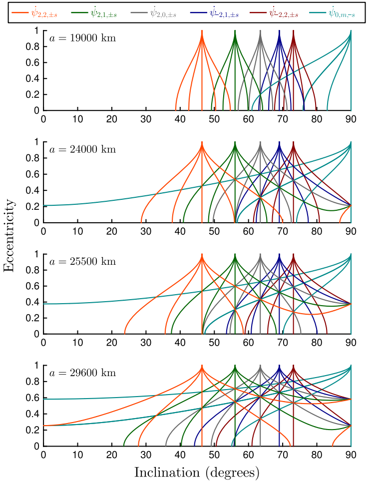

Sun

Fig. 2 Lunisolar resonance centers (*solid lines*) and widths (*transparent shapes*) for increasing values of the satellite's semi-major axis. This *plot* shows the regions of overlap between distinct resonant harmonics

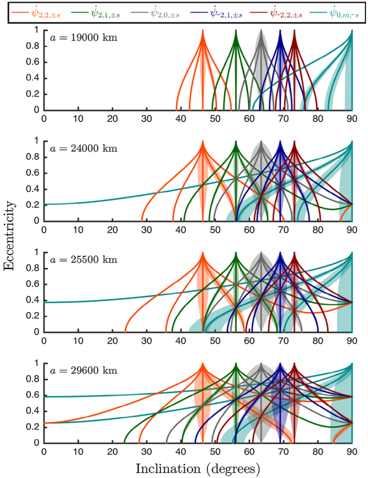

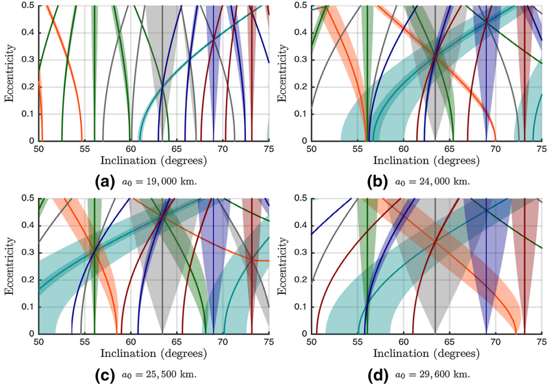

Fig. 3 Zoomed-in portion of Fig. 2, showing where we concentrate our numerical calculations

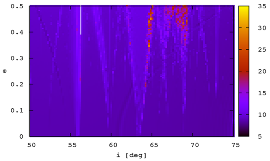

(a) $a_0 = 19,000$ km.

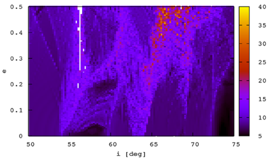

(b) $a_0 = 24,000$ km.

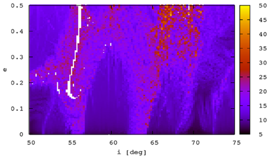

(c) $a_0 = 25,500$ km.

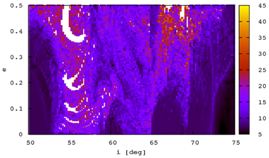

(d) $a_0 = 29,600$ km.

Fig. 4 FLI stability maps for dynamical model 1

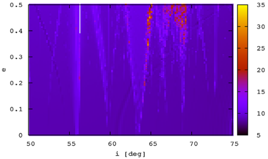

(a) $a_0 = 19,000$ km.

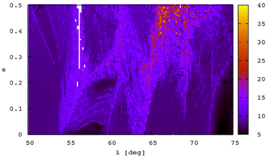

(b) $a_0 = 24,000$ km.

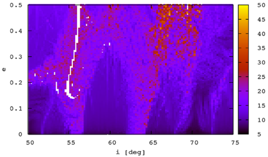

(c) $a_0 = 25,500$ km.

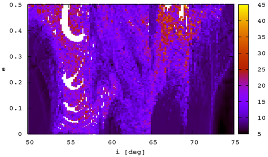

(d) $a_0 = 29,600$ km.

Fig. 4 FLI stability maps for dynamical model 1

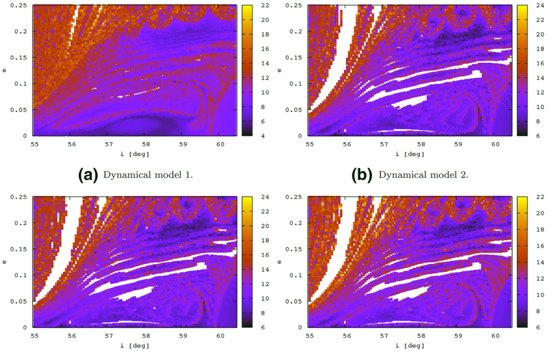

(a) Dynamical model 1.

(b) Dynamical model 2.

(c) Dynamical model 3.

(d) Dynamical model 4.

Fig. 8 Zoomed-in portion for $a_0 = 24,000$ km near the $2\dot{\omega} + \dot{\Omega}$ inclination-dependent-only resonance under the various dynamical models. Initial conditions have been propagated from the initial epoch 2 March 1969 until the final date set to 15 November 2598. The precise detection of the stable manifolds allows to predict the set of re-entry orbits. These maps also further corroborate model 2 as the basic physical model

- Structures on the last plots corresponding to $\sigma_{sec} = 2\omega + \Omega$.
- Secondary resonances : no answer yet ..
- Analogy with other chaos représentations in other fields
- Resonance between σ_{sec} and another angle
- Collaboration between M. Murawiecka and J. Daquin

Paper : *Diffusive chaos in navigation satellites orbits* Daquin, Rosengren]and Tsiganis

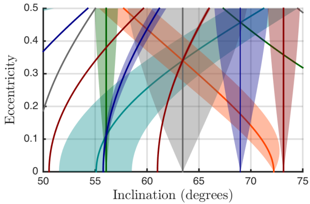

FIGURE 2. Lunisolar resonance centers $\mathcal{C}_{\mathbf{n}}$ (solid lines) and widths $\mathcal{W}_{\mathbf{n}}^{\pm}$ (transparent shapes) for $a_{\star} = 29,600$km, *i.e.*, Galileo's nominal semi-major axis. This plot shows the overlap between the first resonant harmonics ($|n_i| \leq 2, i = 1, \cdots, 3$). Galileo satellites are located near $i = 56°$.

- Celletti and Gales *A study of the lunisolar secular resonance* $2\dot{\Omega} + \dot{\omega} = 0$, Front. Astron. Space Sci., 2016.
- Celletti, Efthymiopoulos, Gachet, Gales and Pucacco *Dynamical models and the onset of chaos in space debris*, JNLM, 2017

Definition 5. A solar semi–secular resonance occurs whenever

$$(l - 2p)\dot{\omega} + m\dot{\Omega} - (l - 2h + j)\dot{M}_S = 0,$$
$$l \in \mathbb{Z}_+,\ m, p, h = 0, 1, 2, \ldots, l,\ j \in \mathbb{Z}.$$

We have a lunar semi–secular resonance whenever

$$(l - 2p)\dot{\omega} + m\dot{\Omega} \pm [(l - 2q)\dot{\omega}_M + (l - 2q + r)\dot{M}_M + s\dot{\Omega}_M] = 0,$$
$$l \in \mathbb{Z}_+,\quad m, p, q, s = 0, 1, 2, \ldots, l,\quad r \in \mathbb{Z}.$$

drag

- LEO region : complete dynamics up to reentry
- Atmospheric drag or cleaner of space junk
- Different models and approaches
- Petit and Lemaitre ASR
- Included in NIMASTEP

Density models

- JB2008 : Jacchia-Bowman 2008, semi-analytical model, based on Jacchia-71 - Reference of Committee on Space Research (COSPAR)
- DTM2013 : Drag Temperature Model, semi-analytical model , including data of the satellites Stella, Starlette, OGO-6, DE-2, AE-C, AE-E, CHAMP, GRACE and GOCE for altitudes between 200 and 900 km,
- TD88 : empirical model, filled on the observation data, extended up to 1200 kms
- Other versions of Jacchia, MSIS, NRLMSISE00, GRAM, MET, GOST, TIEGCM
- Density functions depend on solar flux, geomatic activity, local time, length of the day, latitude.

Comparisons

- Comparison of the models with a real orbit
- TLE of 2 satellites : Stella and Starlette
- NIMASTEP - Adam-Bashforth-Moulton order 10
- More than 20 years

CPU time for Stella

· Temps de calcul des orbites de Stella avec différents modèles d'atmosphère.

	JB2008	DTM2013	TD88
Time	58′32″	15′19″	6′31″

Starlette

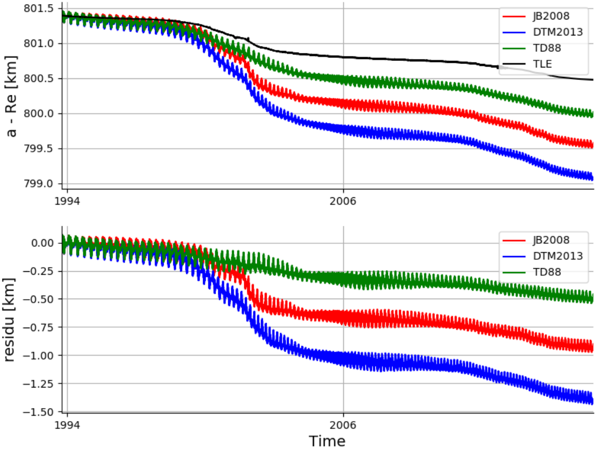

FIGURE 6.5 – Evolution du demi-grand axe du satellite Starlette calculé avec les modèles JB2008, DTM2013, et TD88, et comparé aux pseudo-observations TLE.

Stella

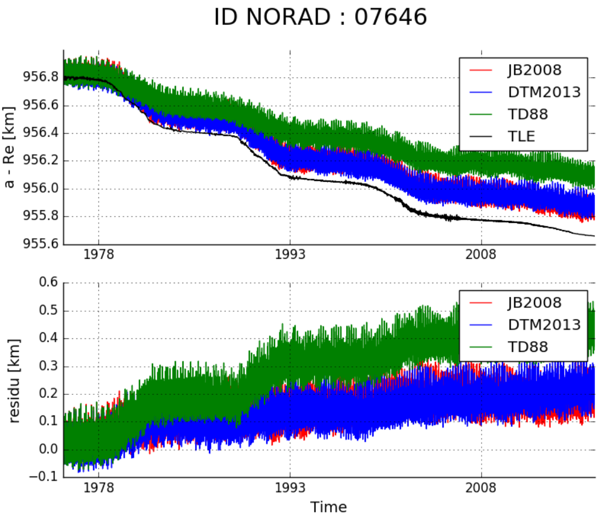

FIGURE 6.6 – Evolution du demi-grand axe du satellite Stella calculé avec les modèles JB2008, DTM2013, et TD88, et comparé aux pseudo-observations TLE.

Chinese satellite explosion

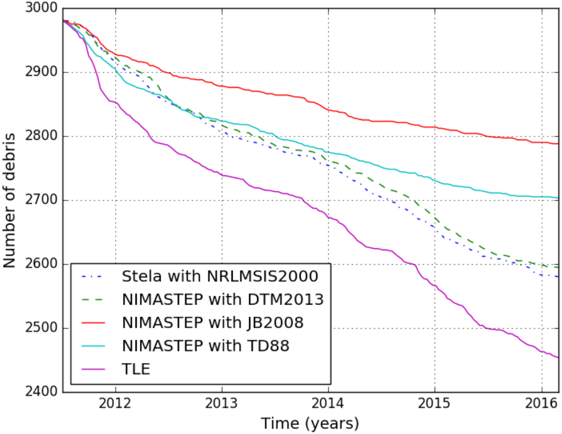

FIGURE 8.4 – Evolution du nuage de débris spatiaux créés par la fragmentation du satellite Fengyun 1C et catalogués par l'USSTRATCOM à la date du premier juin 2011.

Collision Cosmos-Iridium

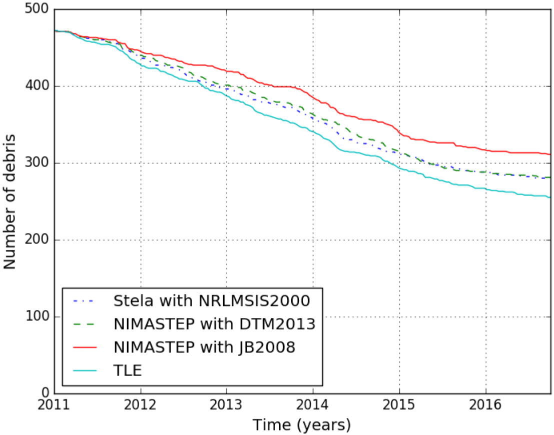

FIGURE 8.5 – Evolution du nuage de débris spatiaux créés par la fragmentation du satellite Iridium 33 et catalogués par l'USSTRATCOM à la date du premier juin 2011.

Yarkovsky-Schachs effect

- Classical formulations
- Thermal effect : differences of temperature of the satellite due to the Sun
- The Yarkovsky-Schachs effect : long-term semi-major axis variations only when the orbit crosses Earth shadow
- The solar flux arriving at the satellite surface is interrupted, the satellite surface cools down after entering the shadow, and heats up again after exiting from it.
- The recoil force does not average out one orbit, the problem becomes therefore position-dependent.
- Poster of M. Murawiecka

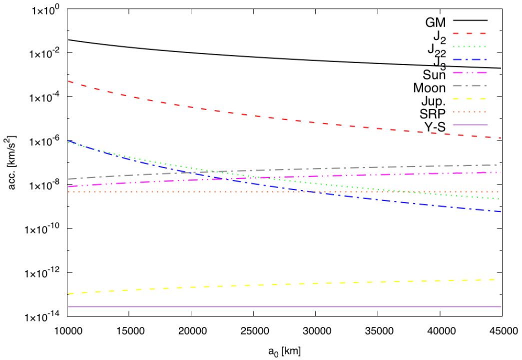

Figure 1: Order of magnitude of several major Earth satellite perturbations as a function of semi-major axis of the orbit.

Semi-major axis

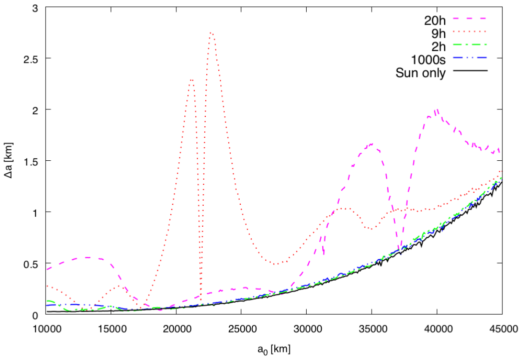

Figure 2: Comparison of amplitude of semi-major axis variations Δa depending on its initial value with various rotation periods of the debris. The initial values of remaining elements are: $e = 0.01$, $i = 0.01^{\circ}$, $\Omega = \omega = M = 0.0^{\circ}$. Rotation periods: magenta – 20h, red – 9h, green – 2h, blue – 1000s. The black curve marks the orbits under the influence of the Sun alone. The simulation time is 400y.

Rotation periods

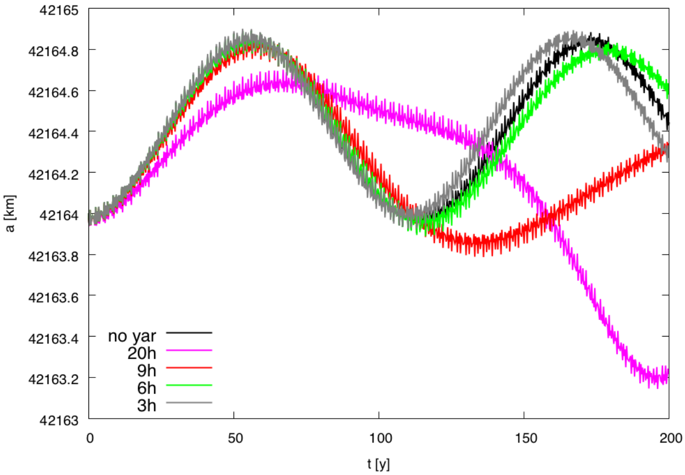

Figure 3: Time evolution of the orbits of a space debris affected by Sun gravity (black curve) or Sun gravity and the Yarkovsky-Schach effect, with various rotation periods

Eccentricity

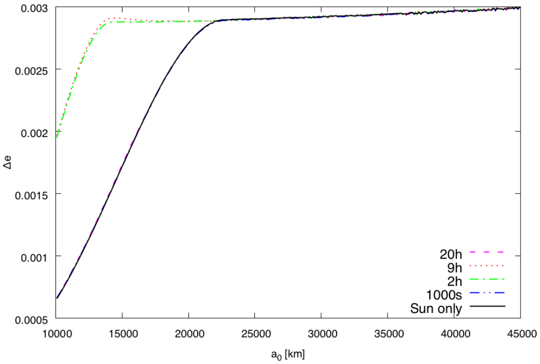

Figure 6: Variations in eccentricity as a funtion of the initial value of the semi-major axis with various rotation periods of the debris. All the initial values of the orbital elements are the same as in Fig. 2. Rotation periods: magenta – 20h, red – 9h, green – 2h, blue – 1000s. The black curve representing Sun-induced variations coincides with the violet one. The integration time is 200 y.

Synthetic population

- naXys Institute : Namur Complex systems
- research group : mobility, traffic : projects since 40 years
- from Dijkstra algorithm of shortest paths in a graph to psychological models about human behaviour
- Necessity of data about families, schools, supermarkets, employed or not, etc
- Some data, locally obtained and big protection of private life
- Last ten years : building of a synthetic population of Belgians, 10 millions of people, organised in families, with work, schools, habits, completely virtual but as close as possible to the reality (the available local data)
- Expertise in specific statistical methods adapted to this problem

Analogy

- 20 000 TLE corresponding to 10 cm or more objects
- Objects of 1 cm ?
- To create a synthetic population with virtual objects, with similar characteristics to the real ones
- Objective : simulation of an event (explosion, collision) and predictions about the debris cloud
- Collaboration of two Phd of different teams : A. Petit and M. Dumont
- First results

Debris synthetic population

- Method : Iterative Proportional Fitting (IPF) : iterative process for weighting data describing a population up to the convergence to a stable state
- Matrix formulation : discretization of the data $(a, e, i, \omega, \Omega, M, A/M)$
- First promising results

Initial population and synthetic population

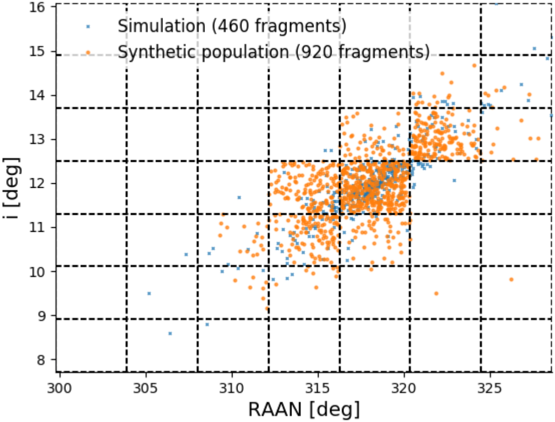

FIGURE 10.3 – Réprésentation de la population simulée (en bleu) et de la population synthétique (en orange).

Convergence of the method

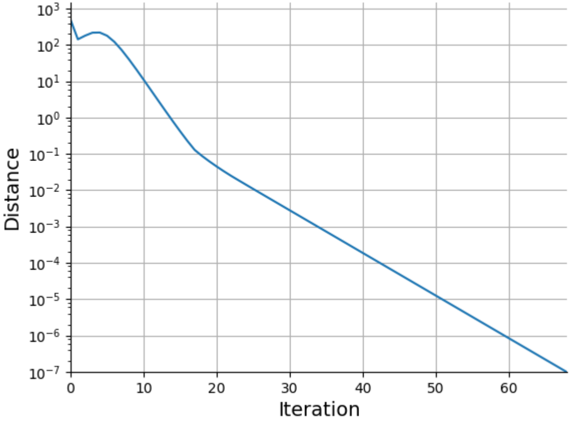

FIGURE 10.4 – Evolution de la distance entre deux table de contingence à chaque itération.

Fragmentation of satellite Ekran 2

Initial population + diminution ejection velocity (factor 10)

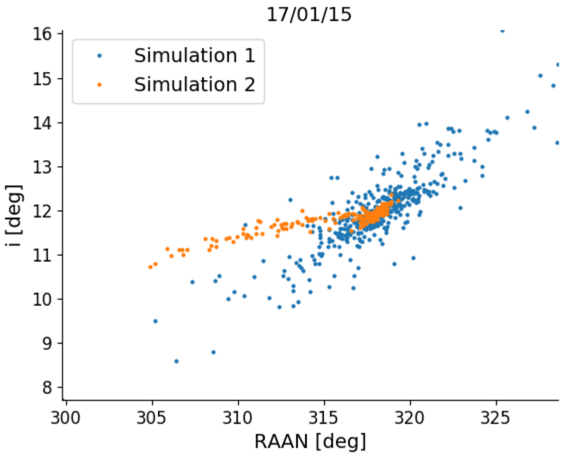

FIGURE 10.5 – Comparaison entre la première simulation avec les incréments de vitesse nominaux et seconde simulation avec les incréments de vitesse divisé par un facteur 10.

Difference between the two populations

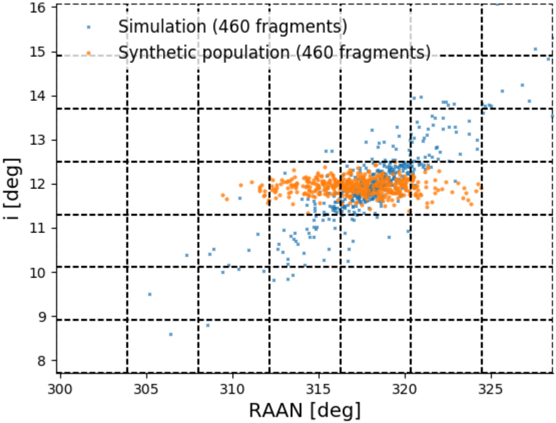

FIGURE 10.6 – Réprésentation de la population simulée (en bleu) et de la population synthétique (en orange).